AGU PUBLICATIONS

Geophysical Research Letters

RESEARCH LETTER
10.1002/2016GL070413

Key Points:
- Observed oceanic heat uptake (33 ± 21 TW) below 2000 m during 1991–2010, majority (2/3) in deep layer (2000–4000 m)
- Temperature trends larger with lower uncertainty in the abyss (4000–6000 m) than in the deep (2000–4000 m) ocean
- Global warming rate did not significantly change from the 1990s to the 2000s but significant variability regionally

Correspondence to:
D. G. Desbruyères,
dades@noc.ac.uk

Citation:
Desbruyères, D. G., S. G. Purkey, E. L. McDonagh, G. C. Johnson, and B. A. King (2016), Deep and abyssal ocean warming from 35 years of repeat hydrography, *Geophys. Res. Lett.*, *43*, 10,356–10,365, doi:10.1002/2016GL070413.

Received 12 JUL 2016
Accepted 14 SEP 2016
Accepted article online 17 SEP 2016
Published online 9 OCT 2016

Deep and abyssal ocean warming from 35 years of repeat hydrography

Damien G. Desbruyères[1], Sarah G. Purkey[2,3], Elaine L. McDonagh[1], Gregory C. Johnson[4], and Brian A. King[1]

[1]National Oceanography Centre, Southampton, UK, [2]Lamont-Doherty Earth Observatory, Columbia University, New York, New York, USA, [3]Scripps Institution of Oceanography, University of California, San Diego, La Jolla, California, USA, [4]NOAA/Pacific Marine Environmental Laboratory, Seattle, Washington, USA

Abstract Global and regional ocean warming deeper than 2000 m is investigated using 35 years of sustained repeat hydrographic survey data starting in 1981. The global long-term temperature trend below 2000 m, representing the time period 1991–2010, is equivalent to a mean heat flux of 0.065 ± 0.040 W m^{-2} applied over the Earth's surface area. The strongest warming rates are found in the abyssal layer (4000–6000 m), which contributes to one third of the total heat uptake with the largest contribution from the Southern and Pacific Oceans. A similar regional pattern is found in the deep layer (2000–4000 m), which explains the remaining two thirds of the total heat uptake yet with larger uncertainties. The global average warming rate did not change within uncertainties pre-2000 versus post-2000, whereas ocean average warming rates decreased in the Pacific and Indian Oceans and increased in the Atlantic and Southern Oceans.

1. Introduction

Quantifying and understanding regional patterns and the mechanisms controlling global energy and sea level budgets is a major scientific challenge. The global ocean absorbs the vast majority (93%) of the planetary energy imbalance, with the remaining 7% accounted for by land warming, atmosphere warming and moisture gain, and melting ice [*Rhein et al.*, 2013]. However, much of the ocean volume remains unmonitored or sparsely sampled in space and time [*Lyman and Johnson*, 2013], and historical estimates of ocean heat content (OHC) prior to the mid-2000s are mostly limited to the upper 700 m [e.g., *Abraham et al.*, 2013]. The Argo array has now yielded more than a decade (2006–2016) of crucial information on OHC shallower than 2000 m [*Roemmich et al.*, 2015; *Wijffels et al.*, 2016]. Argo's extension toward the ocean bottom promises to yield unprecedented insights into the poorly known behavior of the deep (2000–4000 m, herein) and abyssal (below 4000–6000 m) oceans. However, until the Deep Argo array approaches its targeted strength of 1200 active full-depth profiling floats [*Johnson et al.*, 2015], decadal repeats of hydrographic sections [*Talley et al.*, 2016] will be the only global-scale observing system for the deep and abyssal ocean.

The ocean below 2000 m is filled with water masses formed at high latitudes via air-sea and ocean-ice interaction, deep convection, and deep overflows. Open water convection in the Labrador Sea and deep overflows from the Nordic Seas form the North Atlantic Deep Water (NADW), which feeds into the southward flowing limb of the Meridional Overturning Circulation (MOC). This water mass overlies the northward flowing Antarctic Bottom Water (AABW) that covers a substantial fraction of the global ocean bottom [*Johnson*, 2008]. AABW is formed in the Southern Ocean when cold, dense shelf waters cascade down the continental slope and mix with ambient waters [*Gordon*, 2001]. NADW and AABW communicate high-latitude changes throughout the globe, by affecting the large-scale, density-driven ocean circulation and contributing to global energy storage.

Using repeat hydrographic section data taken between 1981 and 2010, *Purkey and Johnson* [2010] quantified heat storage trends below 2000 m within 32 deep ocean basins around the globe. They identified a clear southern intensified warming pattern, with a global OHC increase of 0.068 ± 0.061 W m^{-2} below 2000 m and 0.030 ± 0.009 W m^{-2} below 4000 m, mostly owing to a warmer Lower Circumpolar Deep Water and AABW. Recent analyses of individual sections suggest that the past decade witnessed substantial variability of NADW

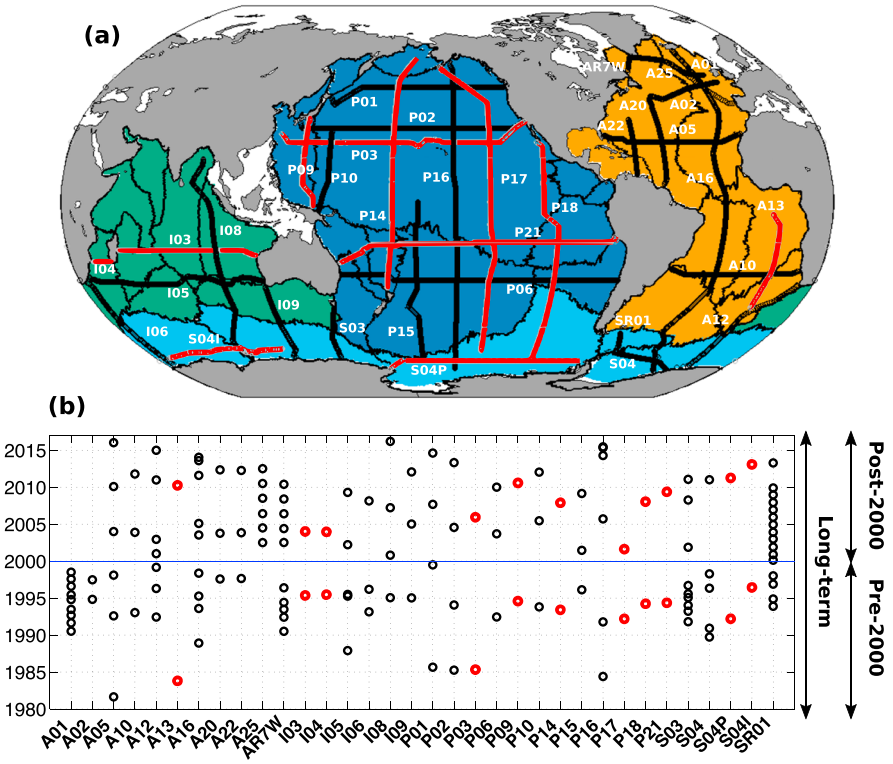

Figure 1. (a) Locations of repeated hydrographic sections with WOCE-designated IDs and (b) their dates of occupations. Red lines and circles indicate those section repeats not included in the pre-2000, post-2000, and long-term S1 estimates (see text for details). Basins are grouped into Atlantic (orange), Pacific (dark blue), Indian (green), and Southern (light blue).

[*Desbruyères et al.*, 2014] and AABW [*Johnson et al.*, 2014], implying regional and possibly global decadal variations of the global deep ocean warming pattern.

Here we update the data through 2015 (section 2) to extend *Purkey and Johnson*, 2010's [2010] long-term analysis and investigate decadal deep and abyssal ocean temperature changes on global (section 3.1) and ocean (section 3.2) scales by analyzing trends during pre-2000 and post-2000 time periods where data coverage is sufficient. Results are then summarized and discussed (section 4).

2. Data and Methods

We use high-quality deep ocean temperature, salinity, and pressure data from all shipboard repeated hydrographic sections publically available as of April 2016 at http://cchdo.ucsd.edu/. These sections were mostly first sampled in the 1990s through the international World Ocean Circulation Experiment (WOCE) Hydrographic Program, a full-depth, global, high-resolution oceanographic survey producing a baseline for the deep ocean's hydrographic properties. Subsequently, a subset of the WOCE sections has been reoccupied in support of the Climate Variability and Predictability (CLIVAR) and Carbon Cycle Science programs, now coordinated by the international Global Ocean Ship-Based Hydrographic Investigations Program (GO-SHIP).

Temperature, salinity, and pressure profiles with accuracy better than 0.002°C, 0.002 PSS-78, and 3 dbar, respectively [*Hood et al.*, 2010] were collected from the surface to a depth of 10–20 m from the bottom using a conductivity-temperature-depth (CTD) instrument, nominally every 55 km along each section. The temperature and salinity data were binned into 1 or 2 dbar pressure bins during initial processing. The global data set consists of 148 hydrographic sections repeated along 34 cruise tracks spanning 1981 to 2016 (Figure 1). Most of the 33 bathymetry-defined deep ocean basins are reasonably sampled (note that the Scotia Sea basin was not included in *Purkey and Johnson* [2010]), with exceptions in the easternmost Pacific Basins and in the northwestern Indian Ocean (Figure 1a). For the analysis below, these basins are assembled into four groups: Atlantic (orange), Pacific (dark blue), Indian (green), and Southern (light blue).

Mean temperature trends on isobars below 2000 m are estimated for each basin. Along each hydrographic section, quality-controlled temperature data are linearly interpolated onto a 20 dbar vertical and 2 min horizontal grid. Linear interpolation is then used to construct a yearly time series of temperature at each grid point from the first to the last section repeat, allowing computation of temperature changes $\frac{d\theta}{dt}$ from a linear model fitted over the chosen time periods (see below). The mean $\frac{d\theta}{dt}$ and its standard deviation $\sigma_{\frac{d\theta}{dt}}$ at every pressure level are obtained for each of the basins by dividing the sections at the basin boundaries. If a basin is crossed by more than one section, the section length-weighted average and standard deviation are used. If measurements do not extend to the deepest portion of the basin, the deepest estimates of $\frac{d\theta}{dt}$ and $\sigma_{\frac{d\theta}{dt}}$ are replicated down to the seafloor. The number of degrees of freedom (DOF) for a given basin is the sum of the lengths of portions of any sections crossing that basin divided by $L = 163$ km, which is our best estimate of the horizontal decorrelation scale for all sections longer than 2000 km at all pressures [*Purkey and Johnson*, 2010]. Note that using a global mean L may decrease the number of DOF at high latitudes where L is likely smaller than 163 km, possibly causing a slight overestimate of the errors in these regions. Yet given the sparse hydrography sampling, we could not distinguish the dependence of L on latitude with any statistical confidence. The uncertainty of the mean $\frac{d\theta}{dt}$ at every pressure level for each basin is computed by dividing the mean $\sigma_{\frac{d\theta}{dt}}$ by the square root of the total number of DOF of that basin. All uncertainties herein are a 5–95% confidence intervals of trends assuming Student's t distribution. The area of each basin at each pressure level is then used as a weight to compute five distinct temperature trend profiles for the Atlantic Ocean, Pacific Ocean, Indian Ocean, Southern Ocean, and global ocean (Figure 2), with zero warming rates prescribed to unsampled basins. Prescribing the global average trend to unsampled basins yields very similar quantitative results. Due to a lack of deep repeat hydrographic data, the Arctic Ocean is not included in the analysis.

Basin, ocean, and global mean temperature trends and their associated uncertainties are computed over three temporal windows. The "long-term" estimate, which uses all hydrographic repeats between 1981 and 2016 (Figure 1b), is an update of that made by *Purkey and Johnson* [2010]. In addition, temperature trends are estimated for two shorter time spans running until and from the year 2000, referred to as the "pre-2000" and the "post-2000" estimates, respectively. These shorter temporal windows reduce the number of available sections and hence the spatial coverage. Eleven sections having only one occupation during each of the shorter time frames (Figure 1a, red lines) are excluded for both the pre-2000 and post-2000 estimates. For the remaining 23 sections, the year 2000 is used as a breaking point for computing pre-2000 and post-2000 temperature changes from a linear model fit. In order to assess the potential biases introduced by excluding 11 sections in pre-2000 and post-2000, a twin long-term estimate (referred to as "long-term S1") is performed using only the 23 sections used in the pre-2000 and post-2000 trend estimates (Figure 1a, black lines). The difference between the long-term and the long-term S1 reflects a bias from undersampling during the pre-/post-2000 time periods. It is referred to as the "sampling bias" hereafter and is considered as an additional error estimate for the pre-2000 and post-2000 trends, in conjunction with the 95% confidence intervals calculated from the regional variance. For each basin, a representative time span is computed by averaging the dates of the first and last occupations of all sections used for that particular basin (Table 1). Hence, the time spans describing the long-term, pre-2000, and post-2000 estimates differ slightly among basins.

We compute for each basin the local heat content trend (Q_i) and the thermosteric sea level rise (η_i) implied by the warming rate below an isobath i, using mean profiles of density (ρ), heat capacity (C_p), and thermal expansion (α) coefficients from the World Ocean Atlas 2013 climatology product [*Boyer et al.*, 2013]:

$$Q_i = \frac{1}{a_i} \int_{z=i}^{z=6000} \rho C_p \frac{d\theta}{dt} a dz \tag{1}$$

$$\eta_i = \frac{1}{a_i} \int_{z=i}^{z=6000} \alpha \frac{d\theta}{dt} a dz \tag{2}$$

where a is the surface area of each individual 20 m spaced isobath z calculated from the ETOPO2.v2 bathymetry product. In section 3, we will provide the local quantification of Q and η for the deep (2000–4000 m), the abyssal (4000–6000 m), and the total (2000–6000 m) layers, as well as their contribution to the global heat and sea level budgets. The standard errors are computed from the volume-weighted variance of Q and η and the volume-weighted DOF within the three layers, using a as a weight in the

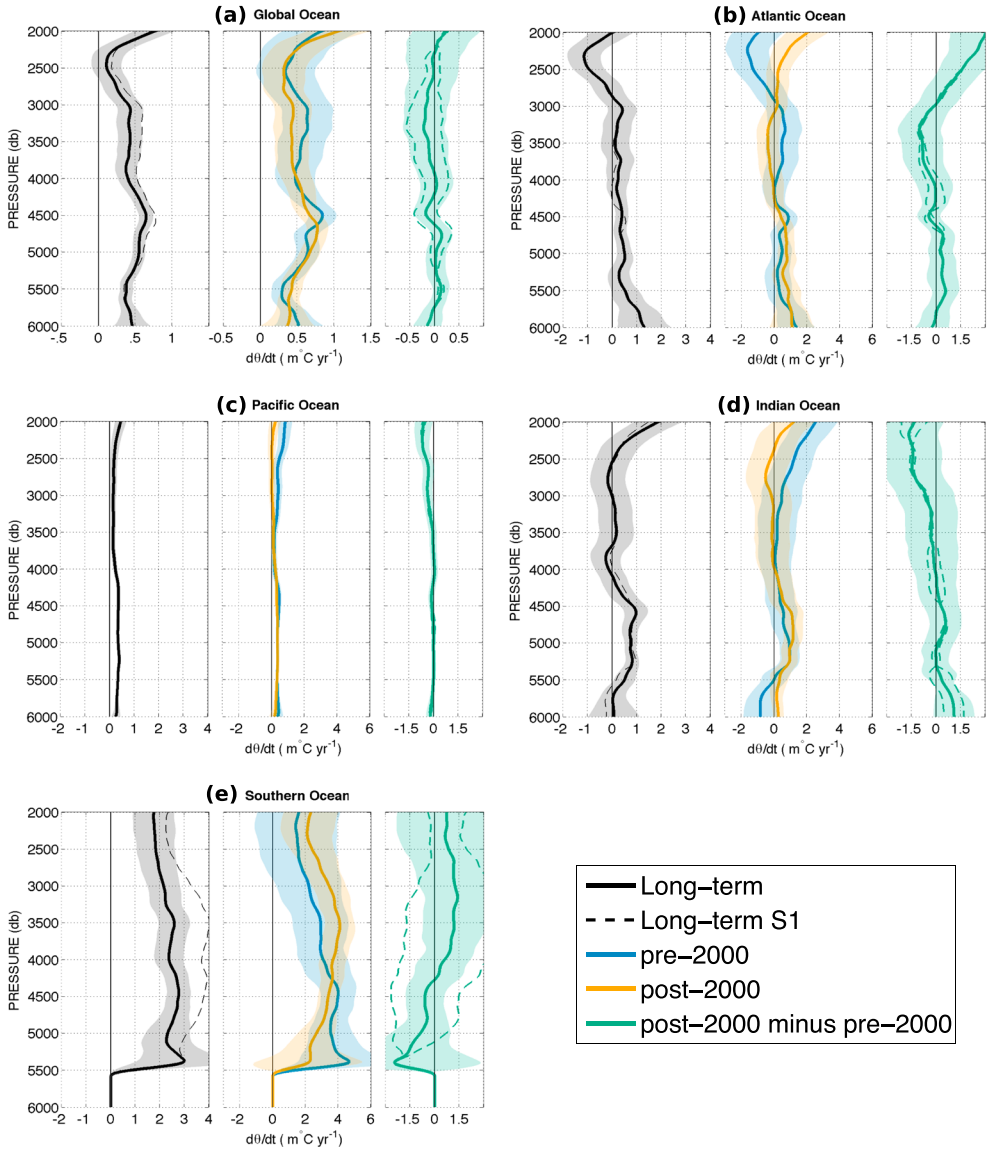

Figure 2. Mean temperature trends $\frac{d\theta}{dt}$ (in m °C yr^{-1}) versus pressure for the (a) global ocean, (b) Atlantic Ocean, (c) Pacific Ocean, (d) Indian Ocean, and (e) Southern Ocean for the long-term estimate (black), the long-term S1 estimate (dashed black), the pre-2000 estimate (blue), the post-2000 estimate (orange), and the difference between post-2000 and pre-2000 (green). The 95% confidence intervals are shown shaded. Twice the difference between long-term and long-term S1 gives an independent uncertainty range for the decadal change (dashed green; see text for details). Time-mean periods described by the long-term profiles are provided in Table 1.

vertical integration. The 95% confidence intervals are finally obtained assuming Student's *t* distribution. Due to the similar characteristics of the heat content and thermosteric sea level trend patterns, only the former is described in section 3. The thermosteric sea level trends and their implications for the global sea level budget are discussed in section 4.

3. Results

3.1. Global Trend

The long-term (1991–2010) global temperature trend reveals warming at all pressure levels below 2000 m, with the largest values observed approximately 2000 m (Figure 2a, black). The mean warming rate between 2000 m depth and the seafloor is 0.39±0.17 m °C yr^{-1}, equivalent to a global heat gain of 33±21 TW, or a mean

Table 1. The Heat Content Trends Q (in TW) Required to Explain Observed Temperature Changes Within the Total 2000–6000 m Layer, the Deep 2000–4000 m Layer, and the Abyssal 4000–6000 m Layer[a]

OHC	Global Long Term (1991–2010)	Atlantic Long Term (1991–2010)	Pacific Long Term (1991–2010)	Indian Long Term (1992–2008)	Southern Long Term (1992–2012)
Total	33 ± 21	−1 ± 13	10 ± 7	4 ± 12	21 ± 7
Deep	22 ± 21	−3 ± 13	6 ± 7	2 ± 12	17 ± 7
Abyssal	11 ± 3	2 ± 2	4 ± 1	2 ± 2	4 ± 1
	Pre-2000 (Post-2000)	Pre-2000 (Post-2000)	Pre-2000 (Post-2000)	Pre-2000 (Post-2000)	Pre-2000 (Post-2000)
Total	47 ± 41 (±9)	−3 ± 24 (±0)	17 ± 15 (±0)	11 ± 19 (±0)	23 ± 23 (±10)
	42 ± 32 (±9)	4 ± 18 (±1)	6 ± 11 (±0)	1 ± 21 (±0)	31 ± 12 (±10)
Deep	34 ± 42 (±7)	−5 ± 24 (±1)	13 ± 15 (±0)	9 ± 19 (±0)	17 ± 23 (±8)
	29 ± 32 (±7)	3 ± 19 (±1)	2 ± 11 (±0)	−1 ± 21 (±0)	25 ± 12 (±8)
Abyssal	13 ± 6 (±2)	1 ± 4 (±1)	4 ± 2 (±0)	2 ± 3 (±0)	6 ± 2 (±2)
	13 ± 6 (±2)	2 ± 4 (±1)	3 ± 1 (±0)	2 ± 3 (±0)	5 ± 1 (±2)
SLR	Global Long Term (1991–2010)	Atlantic Long Term (1991–2010)	Pacific Long Term (1991–2010)	Indian Long Term (1992–2008)	Southern Long Term (1992–2012)
Total	1.17 ± 0.73	−0.05 ± 0.48	0.36 ± 0.24	0.14 ± 0.44	0.72 ± 0.23
Deep	0.70 ± 0.74	−0.11 ± 0.49	0.20 ± 0.25	0.06 ± 0.44	0.54 ± 0.23
Abyssal	0.46 ± 0.13	0.06 ± 0.08	0.16 ± 0.04	0.07 ± 0.08	0.17 ± 0.04
	Pre-2000 (Post-2000)	Pre-2000 (Post-2000)	Pre-2000 (Post-2000)	Pre-2000 (Post-2000)	Pre-2000 (Post-2000)
Total	1.66 ± 1.41 (±0.32)	−0.11 ± 0.88 (±0.04)	0.59 ± 0.50 (±0.01)	0.37 ± 0.67 (±0.02)	0.81 ± 0.72 (±0.34)
	1.50 ± 1.11 (±0.32)	0.15 ± 0.66 (±0.04)	0.24 ± 0.36 (±0.01)	0.06 ± 0.73 (±0.02)	1.05 ± 0.38 (±0.34)
Deep	1.11 ± 1.44 (±0.24)	−0.17 ± 0.90 (±0.03)	0.42 ± 0.50 (±0)	0.31 ± 0.68 (±0.01)	0.56 ± 0.73 (±0.27)
	0.95 ± 1.14 (±0.24)	−0.08 ± 0.69 (±0.03)	0.08 ± 0.36 (±0)	−0.03 ± 0.74 (±0.01)	0.83 ± 0.39 (±0.27)
Abyssal	0.54 ± 0.26 (±0.08)	0.08 ± 0.19 (±0.01)	0.15 ± 0.07 (±0.01)	0.07 ± 0.12 (±0.02)	0.24 ± 0.09 (±0.07)
	0.54 ± 0.24 (±0.08)	0.07 ± 0.20 (±0.01)	0.15 ± 0.06 (±0.01)	0.09 ± 0.12 (±0.02)	0.22 ± 0.05 (±0.07)

[a]The top table shows long-term estimates, and the bottom table shows pre-2000 and post-2000 estimates. The 95% confidence levels are given. For the each estimate, the time-mean period represented by the observed trend is indicated. Alternative uncertainties for pre-2000 and post-2000 (shown in parentheses) are obtained from the difference between the long-term estimate and the long-term S1 estimate (see text for details). SLR is same as OHC for steric sea level rise η for the global ocean (in mm decade^{-1}).

downward heat flux of 0.065 ± 0.040 W m^{-2} over the Earth's surface area. The trend values are statistically significant at every pressure level (except approximately 2500 m where the temperature trend approaches zero) and the uncertainty decreases with depth along with the spatial variability. The deep (2000–4000 m) and abyssal (4000–6000 m) layers show mean warming rates of 0.34 ± 0.19 m °C yr^{-1} and 0.53 ± 0.11 m °C yr^{-1} and explain 67% (22 ± 21 TW) and 33% (11 ± 3 TW) of the global ocean heat gain below 2000 m depth, respectively. For both layers, the dominant role of the Southern Ocean stands out from the global pattern of heat content trends (Figures 3a and 3b).

The aforementioned values represent an update of *Purkey and Johnson*, 2010's [2010] analysis using 38 additional repeats mostly carried out after the year 2010. This extended data set does not substantially impact the structure and magnitude of the global trend, previously estimated as 20 ± 26 TW (0.041 ± 0.052 W m^{-2}), 13 ± 4 TW (0.027 ± 0.009 W m^{-2}), and 34 ± 31 TW (0.068 ± 0.061 W m^{-2}) between the 1990s and 2000s for the deep, abyssal, and total layers, respectively [*Purkey and Johnson*, 2010]. This suggests that the deep and abyssal global warming rate has not undergone dramatic changes during the most recent years. However, recomputing the trends over longer time periods using more data does reduce the global uncertainties.

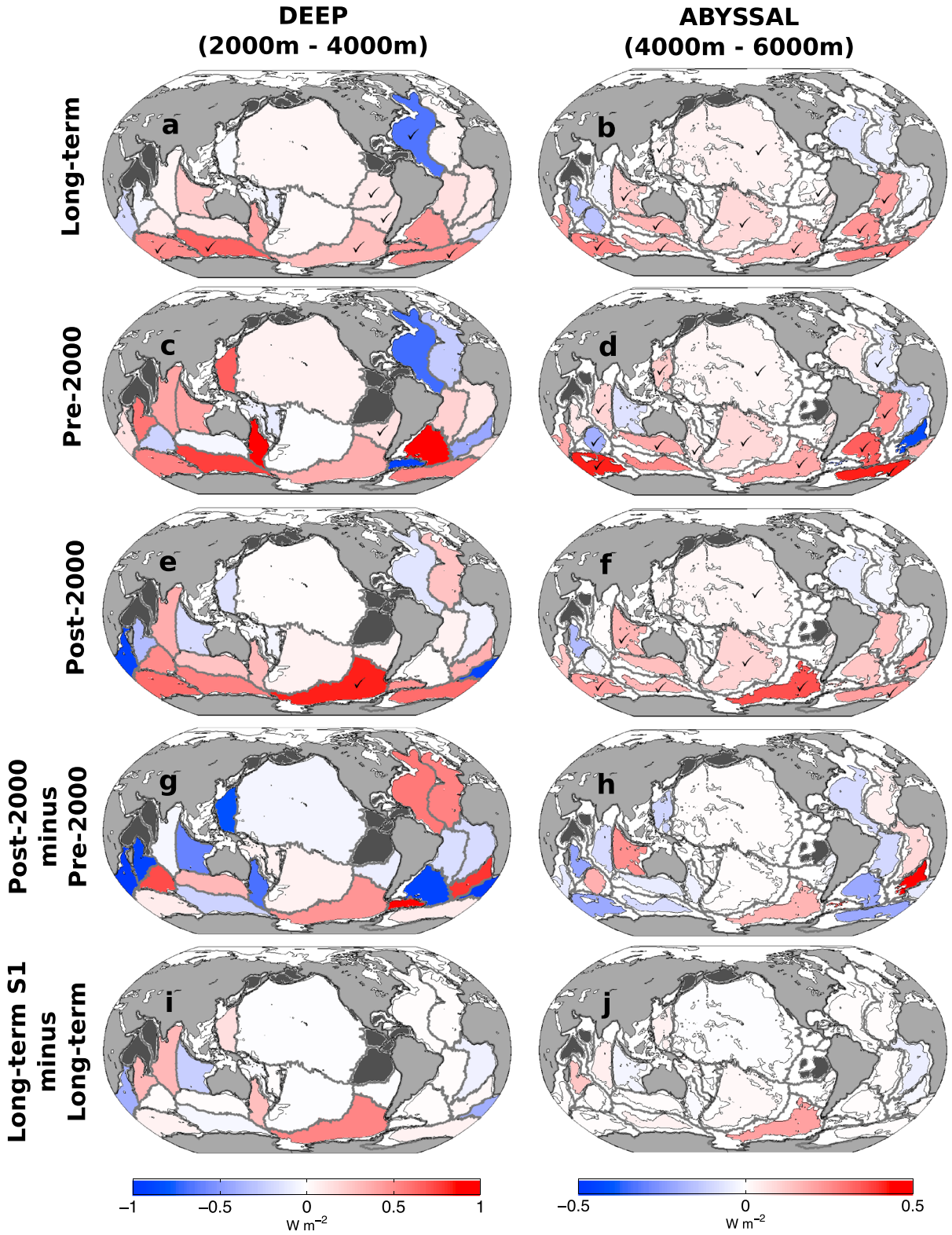

Figure 3. Spatial distributions of local heat content trend Q (in W m^{-2}) within (a, c, e, g, and i) the deep 2000–4000 m layer and (b, d, f, h, and j) the abyssal 4000–6000 m layer from the long-term estimate (Figures 3a and 3b), the pre-2000 estimate (Figures 3c and 3d), the post-2000 estimate (Figures 3e and 3f), the difference between post-2000 and pre-2000 estimates (Figures 3g and 3h), and the difference between the long-term S1 and the long-term estimates (Figures 3i and 3j). Basins colored in black have not been sampled by repeat hydrography during the relevant time span. Tick symbols in Figures 3a–3f highlight the OHC trends statistically different from zero at 95% confidence. Color scale for the deep layer is twice that for the abyssal layer.

Profiles of global temperature trends are consistently similar for the pre-2000 and post-2000 estimates (Figure 2a, blue and orange), with mean warming rates of 0.55 ± 0.35 m °C yr^{-1} (47 ± 41 TW) and 0.49 ± 0.26 m °C yr^{-1} (42±32 TW), respectively. The changes in the magnitude of the trends are not statistically different from zero at the 95% confidence level everywhere below 2000 m. As shown in the following sections, the 5 TW global average change masks large opposing regional variability, with lower warming rates in the Indian Ocean and Pacific Ocean, higher warming rates in the Southern Ocean, and a cooling-to-warming reversal in the Atlantic Ocean.

The pre-2000 and post-2000 global OHC trend magnitudes below 2000 m of 47 ± 41 TW and 42 ± 32 TW, respectively, are slightly higher than the corresponding long-term estimate of 33 ± 21 TW. However, these estimates agree within 95% confidence intervals. The apparent discrepancy arises from the reduced spatial coverage of the hydrographic sections used in pre-2000 and post-2000 estimates. The sampling bias computed from the long-term S1 estimate indicates an increased warming rate between 2500 m and 5000 m (Figure 2a, dashed black line), resulting in an additional 9 TW of uncertainty below 2000 m for the pre-2000 and post-2000 estimates (Table 1). Taken with the measured variability, the discrepancy between the pre-2000 and post-2000 and the long-term OHC trends is well within the total uncertainty (Figure 2a, dashed green lines), suggesting that there has not been a significant change in the total accumulation rates of deep and abyssal OHC for the two different time periods.

3.2. Regional Trends

For each of the three time periods, the global temperature profile is decomposed into its contributions from the Atlantic (Figure 2b), Pacific (Figure 2c), Indian (Figure 2d), and Southern (Figure 2e) Oceans and further into the associated heat content changes within each basin (Figure 3).

3.2.1. Atlantic Ocean

The Atlantic Ocean below 2000 m cooled long-term at a rate of −0.07 ± 0.59 m °C yr^{-1} (−1 ± 13 TW). A significant cooling of its upper deep layer (2000–3000 m) peaking at −1 ± 0.7 m °C yr^{-1} is observed owing to a strong cooling in its northwestern basin (Figure 3a). This is the only basin with a statistically significant cooling trend at deep levels. The remainder of the Atlantic water column below 3000 m underwent a relatively small average warming, which primarily results from warming in the Brazilian and Argentinian Basins, partially offset by abyssal cooling in the north and southeastern basins.

The Atlantic Ocean shows a trend reversal post-2000 in the deep layer (Figure 2b, blue, orange, and green), with a cooling-to-warming tendency between 2000 m and 3000 m (statistically significant shallower than 2500 m) and a warming-to-cooling tendency between 3000 m and 4000 m. The former change occurred in the North Atlantic, while the latter change is observed in the South Atlantic with the strongest contribution from the Argentine Basin, previously reported by *Johnson et al.* [2014] (Figure 3g). Overall, the deep and abyssal OHC variability in the Atlantic Ocean represent a 7 ± 30 TW increase in the global OHC trend (Table 1, top), with a sampling-related uncertainty well within the original uncertainty range (Figure 2b, green dashed lines).

3.2.2. Pacific Ocean

The Pacific Ocean below 2000 m warmed long-term at a rate of 0.23 ± 0.12 m° C yr^{-1} (10 ± 7 TW). The temperature trend indicates warming at every pressure level, with a remarkably smooth vertical structure and small uncertainty range (Figure 2c, black) and a relatively uniform horizontal distribution (Figures 2a and 2b). Despite a relatively small warming rate, this voluminous ocean accounts for almost a third of the global OHC increase below 2000 m (Table 1, top).

The Pacific Ocean shows reduced warming trends post-2000 compared with pre-2000 shallower than 3500 m and no significant variability at abyssal levels (Figure 2c, blue, orange, and green). The warming of the deep layer, which substantially contributed to the global OHC trend during the 1990s (17 ± 15 TW), became smaller during the 2000s (6 ± 11 TW). This decadal decrease of the deep Pacific warming rate is distinguishable from zero at the 95% confidence level shallower than 3500 m and is not driven by sampling-related biases (Figure 3c, dashed). It primarily reflects a small change of the trend magnitude within its voluminous central basin and large changes within the smaller westernmost basins that significantly exceed their associated sampling-related biases (Figure 3i). Overall, the deep and abyssal OHC variability in the Pacific Ocean represents an 11 ± 19 TW decrease in the global OHC trend (Table 1, top). The reduced sampling coverage appears to have no impact on the reported decadal change.

3.2.3. Indian Ocean

The Indian Ocean below 2000 m warmed long term at an average rate of 0.27 ± 0.69 m °C yr^{-1} (4 ± 12 TW), owing to substantial warming trends between 2000 and 2500 m and 4500 and 5500 m (Figure 2d, black).

Warming is predominantly found in the eastern part of the domain and also in the abyssal layer of the Agulhas region, while cooling is detected in the western basins below 4000 m (Figures 3a and 3b).

The Indian Ocean shows reduced and increased post-2000 warming trends shallower and deeper than 3500 m, respectively (Figure 2d, blue, orange, and green), relative to the pre-2000 trends. The deep signal is observed in the eastern and western portions of the domain, while the abyssal signal primarily arises in the easternmost basin. Overall, the deep and abyssal OHC variability in the Indian Ocean represents a 10 ± 28 TW decrease in the global OHC trend (Table 1). Despite the relatively large changes in the deep layer between a strong pre-2000 warming trend and a post-2000 near zero, the large uncertainties of both estimates make their differences undistinguishable from zero at 95% confidence interval. The sampling bias is small over the whole domain and remains within the original uncertainty range (Figure 2d, green dashed lines), but it is locally important at deep levels with cold anomalies within the boundary basins compensating for warm anomaly in the interior (Figure 3i).

3.2.4. Southern Ocean

The Southern Ocean below 2000 m warmed at a long-term rate of 2.17 ± 0.70 m °C yr^{-1} (21 ± 7 TW). This ocean presents a strong and vertically uniform warming through both layers (Figure 2e, black). Despite its relatively small volume, it is the largest contributor to the long-term global heat gain below 2000 m, accounting for 67% of the global trend (Table 1, top). It is also the only region showing an averaged deep (2000–4000 m) heat content trend statistically different from zero at the 95% confidence level. The strong warming rates of the Southern Ocean basins stand out (Figures 3a and 3b), with warming signals suggesting northward spreading into the Pacific Ocean, the southwestern Atlantic Ocean, and the eastern Indian Ocean.

The Southern Ocean shows relatively large differences between the pre-2000 and post-2000 estimates, albeit with relatively large uncertainties (Figure 2e, blue, orange, and green). The mean pre-2000 and post-2000 temperature trends suggest enhanced warming rates shallower than 4500 m primarily owing to increased warming in the Amundsen-Bellingshausen Basin (Pacific sector, Figure 3g) and reduced warming rates below 4500 m owing to the lack of warming in the Weddell-Enderby Basin post-2000 (Indo-Atlantic sector, Figure 3h). Overall, the deep and abyssal OHC variability in the Southern Ocean represent a 8 ± 26 TW increase in the global OHC trend (Table 1, top). The uncertainty of the two estimates is large, and their difference does not reach statistically significant values below 2000 m (Figure 2e, green). Moreover, a relatively large potential sampling bias is revealed in the deep layer (Figure 2e, black and green dashed lines), suggesting that the reported decadal change may include an artifact of sparse data coverage that led to an overestimation of the post-2000 warming rate and/or an underestimation of the pre-2000 warming rate. The first hypothesis appears more likely, as the bias structure closely resembles the post-2000 estimate (Figure 2e, orange), with a peak approximately 3500 m and a sharp transition zone approximately 4300 m. Consequently, the sampling-related uncertainty stands outside the original uncertainty range between 3000 m and 4500 m, making the decadal change indistinguishable from zero. This sampling-related bias is strictly observed in the Amundsen-Bellingshausen Basin, which is consistent with the reduced number of sections available for the pre-2000 and post-2000 calculation within that particular basin (see Figure 1a).

4. Conclusion

Using 148 hydrographic occupations distributed along 34 sections over the global ocean, we make up-to-date estimates of the bidecadal trend in deep (2000–4000 m) and abyssal (4000–6000 m) temperatures on global, ocean, and basin scales and identify any recent reduction, increase, or reversal of those trends between the late 20th and early 21st centuries. Extending *Purkey and Johnson*, 2010's [2010] data set with additional section repeats after 2010 does not significantly change the characteristics of the long-term temperature trend they reported; the global ocean below 2000 m continued to warm at similar rate during the most recent years. However, making the estimate with more data over a longer time period does reduce the uncertainties. The global temperature trend representing the mean period 1991–2010 averages out to 0.39 ± 0.17 m °C yr^{-1} (33 ± 21 TW), which is equivalent to an applied heat flux at the top of the atmosphere of 0.065 ± 0.040 W m^{-2}. This value is about 13% of the total oceanic heat uptake rate estimate between 1993 and 2010 of 257 TW [*Rhein et al.*, 2013] and confirms the predominant storage of anthropogenic heat within the upper half of the ocean in recent decades [*Roemmich et al.*, 2015; *Desbruyères et al.*, 2016], although the deep ocean heat uptake rate is expected to increase with time [*Gleckler et al.*, 2016]. The deep and abyssal ocean warming contributes to a thermosteric sea level rise of 1.17 ± 0.73 mm decade^{-1}, roughly 4% of the total sea level rise of 32 ± 4 mm decade^{-1} over the altimetry period (1993–2012) [*Church et al.*, 2013].

Long-term temperature trends reveal a continued warming of deep and abyssal basins filled by deep waters originating from the Southern Ocean (Figure 3). The bottom limb of the MOC, fed by AABW formed primarily along the Antarctic continental slope, flows north filling the abyssal Pacific, Indian, and South Atlantic and the deep and abyssal Southern Ocean [*Johnson*, 2008]. These regions fed by AABW show uniform and statistically significant warming in the long-term and pre-/post-2000 trends with the exception of the western Indian Ocean. The Southern Ocean warming alone drives 67% of the global long-term heat content rise below 2000 m. This southern intensified global warming of AABW-fed deep and abyssal basins has been connected to a downward isotherm heave—a volume loss of the cold, dense water possibly owing to local changes in AABW production rates around Antarctica, suggesting a slowdown in the bottom limb of the MOC as a potential mechanism [*Purkey and Jonhson*, 2012; *Masuda et al.*, 2010]. Changes in the MOC are also likely to have influenced OHC trends in the North Atlantic, which underwent a strong and statistically significant long-term cooling in the upper deep layer. This cooling, which opposes with the AABW-dominated warming of the global deep ocean, primarily reflects the cold and dense vintage of upper NADW formed in the subpolar gyre during the 1990s [e.g., *Robson et al.*, 2014]. Consistently, previous analysis of repeat hydrography sections highlighted the strong contribution of isopycnal heave to deep temperature trends in the North Atlantic subpolar gyre [*Desbruyères et al.*, 2014].

The additional data used here extended *Purkey and Johnson*'s [2010] deep and abyssal trends beyond 2010 and enabled an investigation of the shorter-term temperature change that occurred during two distinct time periods. The global trends characterizing these two time spans show remarkably similar magnitudes and vertical structures, with the abyss warming at a faster rate than the deep ocean. Within both layers, the difference between pre-2000 and post-2000 trend estimates is indistinguishable from zero at the 95% confidence level. This would imply that no accelerated or attenuated warming was detected in the lower half of the water column during the surface warming slowdown of the 2000s [*Fyfe et al.*, 2016] and that within the large observational uncertainties of the present global deep ocean observing system, the global vertical redistribution of heat expected during such a *hiatus* phenomenon remained confined in the upper half of the water column. This is in line with the analysis of observational products showing a global temperature change between the 1990s and the 2000s restricted above 500 m [*Nieves et al.*, 2015]. Some substantial changes of the temperature trends from one decade to the next are, however, observed in individual oceans, most particularly within the deep layer where the constant global warming rate in pre-2000 and post-2000 is found to result from a compensation between enhanced warming rates in the North Atlantic and Southern Oceans and reduced warming rates in the South Atlantic, Pacific, and Indian Oceans. Among those signals, the statistically significant cooling-to-warming reversal in the deep North Atlantic highlights the general warming of upper NADW observed between the 1990s and the 2000s [e.g., *Yashayaev et al.*, 2007; *Mauritzen et al.*, 2012; *Robson et al.*, 2014]. This reversal reflects a weakening of deep convection in the subpolar gyre, an important mechanism for reducing the rate of global surface warming on decadal timescales [*Meehl et al.*, 2011; *Chen and Tung*, 2014].

Decadal changes of temperature trends are deduced from a reduced data set, with gaps in the section distribution introducing potential biases in the pre-2000 and post-2000 estimates. While estimates in the weakly stratified abyssal layer are barely affected by introducing such spatial gaps in the observing system, a global warm bias accounting for 9 TW is introduced within the deep layer. This bias primarily arises in the Amundsen-Bellingshausen Basin of the Southern Ocean where relatively few hydrographic repeat sections are available. Uncertainties are consequently increased, and the reported intensification of the deep Southern Ocean warming rate is shown not to be significant within these uncertainties.

Reducing uncertainties of the deep and abyssal property changes is one of the main motivations for the launch of deep-profiling Argo floats (the Deep Argo array) capable of recording temperature and salinity below 2000 m at much higher temporal and spatial frequencies than those achieved by shipboard measurements. Its regional implementation has begun in the North Atlantic, Southern Ocean, and southwest Pacific, which is where the largest temperature trends are found. Moving toward the targeted fleet of 1200 floats at 5° × 5° spacing [*Johnson et al.*, 2015], unprecedented information on the formation rates, property changes, and pathways of deep and abyssal water masses will be revealed. However, repeat hydrographic sections, such as those analyzed here, will serve as crucial benchmarks for the development of the array while continuing to provide the most accurate estimates of coast-to-coast full-depth synoptic transports, physical, and biogeochemical properties.

Acknowledgments
This work is a contribution to the DEEP-C project, funded by the British National Environmental Research Council (NERC grant NE/K004387/1). GO-SHIP CTD data were made available by data originators either as public data on the CCHDO website (http://cchdo.ucsd.edu), where cruise participants can be identified, or directly by cruise PIs. We are grateful for the hard work of scientists, ship's officers, and crew in collecting, calibrating, and processing the data used here. G.C.J. is supported by the Climate Observation Division, Climate Program Office, National Oceanic and Atmospheric Administration (NOAA), U.S. Department of Commerce, and NOAA Research. PMEL contribution 4517.

References

Abraham, J. P., et al. (2013), A review of global ocean temperature observations: Implications for ocean heat content estimates and climate change, *Rev. Geophys.*, *51*, 450–483, doi:10.1002/rog.20022.

Boyer, T. P., et al. (2013), World Ocean Database 2013, in *NOAA Atlas NESDIS 72*, edited by S. Levitus and A. Mishonov, pp. 209, U.S. Dep. of Commerce, Silver Spring, Md., doi:10.7289/V5NZ85MT.

Chen, X., and K.-K. Tung (2014), Varying planetary heat sink led to global-warming slowdown and acceleration, *Science*, *345*, 897–903, doi:10.1126/science.1254937.

Church, J. A., et al. (2013), Sea level change, in *Climate Change 2013: The Physical Basis. Contribution of Working Group I to the Fifth Assessment Report of the Intergovernmental Panel on Climate Change*, edited by T. Stocker et al., pp. 1535, Cambridge Univ. Press, Cambridge, U. K., and New York.

Desbruyères, D., E. L. McDonagh, B. A. King, F. K. Garry, A. T. Blaker, B. I. Moat, and H. Mercier (2014), Full-depth temperature trends in the northeastern Atlantic through the early 21st century, *Geophys. Res. Lett.*, *41*, 7971–7979, doi:10.1002/2014GL061844.

Desbruyères, D., E. L. McDonagh, and B. A. King (2016), Observational advances in estimates of oceanic heating, *Curr. Clim. Change Rep.*, *2*, 127–134, doi:10.1007/s40641-016-0037-7.

Fyfe, J. C., et al. (2016), Making sense of the early-2000s warming slowdown, *Nat. Clim. Change*, *6*, 224–228, doi:10.1038/nclimate2938.

Gleckler, P. J., P. J. Durack, R. J. Stouffer, G. C. Johnson, and C. E. Forest (2016), Industrial-era global ocean heat uptake doubles in recent decades, *Nat. Clim. Change*, *6*, 394–398, doi:10.1038/NCLIMATE2915.

Gordon, A. L. (2001), Bottom water formation, in *Encyclopedia of Ocean Sciences*, edited by J. Steel, S. Thorpe, and K. Turekian, pp. 334–340, Elsevier, Amsterdam.

Hood, E. M., C. L. Sabine, and B. M. Sloyan (2010), GO-SHIP repeat hydrography manual: A collection of expert reports and guidelines, *IOCCP Rep. No. 14*. [Available at http://www.go-ship.org/HydroMan.html.]

Johnson, G. C. (2008), Quantifying Antarctic bottom water and North Atlantic deep water volumes, *J. Geophys. Res.*, *113*, C05027, doi:10.1029/2007JC004477.

Johnson, G. C., K. E. McTaggart, and R. Wanninkhof (2014), Antarctic bottom water temperature changes in the western South Atlantic from 1989 to 2014, *J. Geophys. Res. Oceans*, *119*, 8567–8577, doi:10.1002/2014JC010367.

Johnson, G. C., J. M. Lyman, and S. G. Purkey (2015), Informing deep Argo array design using Argo and full-depth hydrography section data, *J. Atmos. Oceanic Technol.*, *32*, 2187–2198, doi:10.1175/JTECH-D-15-0139.1.

Lyman, J. M., and G. C. Johnson (2013), Estimating global ocean heat content changes in the upper 1800 m since 1950 and the influence of the climatology choice, *J. Clim.*, *27*, 1945–1957, doi:10.1175/JCLI-D-12-00752.1.

Masuda, S., et al. (2010), Simulated rapid warming of abyssal North Pacific waters, *Science*, *329*, 319–322, doi:10.1126/science.1188703.

Mauritzen, C., A. Melsom, and R. T. Sutton (2012), Importance of density-compensated temperature change for deep North Atlantic Ocean heat uptake, *Nature Geosci.*, *5*, 905–910, doi:10.1038/ngeo1639.

Meehl, G. A., J. M. Arblaster, J. T. Fasullo, A. Hu, and K. E. Trenberth (2011), Model-based evidence of deep-ocean heat uptake during surface-temperature hiatus periods, *Nat. Clim. Change*, *1*, 360–364, doi:10.1038/NCLIMATE1229.

Nieves, V., J. K. Willis, and W. C. Patzert (2015), Recent hiatus caused by decadal shift in Indo-Pacific heating, *Science*, *349*, 532–535, doi:10.1126/science.aaa4521.

Purkey, S. G., and G. C. Johnson (2010), Warming of global abyssal and deep southern ocean waters between the 1990s and 2000s: Contribution to global heat and sea level rise budgets, *J. Clim.*, *23*, 6336–6350, doi:10.1175/2010JCLI3682.1.

Purkey, S. G., and G. C. Jonhson (2012), Global contraction of Antarctic Bottom Water between the 1980s and 2000s, *J. Clim.*, *25*, 5830–5844, doi:10.1175/JCLI-D-11-00612.1.

Rhein, M., et al. (2013), Observations: Oceans, in *Climate Change 2013: The Physical Science Basis. Contribution of Working Group I to the Fifth Assessment Report of the Intergovernmental Panel on Climate Change*, edited by T. Stocker et al., pp. 255–316, Cambridge Univ. Press, Cambridge, U. K., and New York, doi:10.1017/CBO9781107415324.010.

Robson, J., D. Hodson, E. Hawkins, and R. Sutton (2014), Atlantic overturning in decline?, *Nat. Geosci.*, *7*, 2–3, doi:10.1038/ngeo2050.

Roemmich, D., J. Church, J. Gilson, D. Monselesan, P. Sutton, and S. Wijffels (2015), Unabated planetary warming and its ocean structure since 2006, *Nat. Clim. Change*, *5*, 240–245, doi:10.1038/NCLIMATE2513.

Talley, L. D., et al. (2016), Changes in ocean heat, carbon content, and ventilation: A review of the first decade of GO-SHIP global repeat hydrography, *Annu. Rev. Mar. Sci.*, *8*, 185–215, doi:10.1146/annurev-marine-052915-100829.

Wijffels, S., D. Roemmich, D. Monselesan, J. Church, and J. Gilson (2016), Ocean temperatures chronicle the ongoing warming of Earth, *Nat. Clim. Change*, *6*, 116–118, doi:10.1038/nclimate2924.

Yashayaev, I., M. Bersh, and H. M. van Aken (2007), Spreading of the Labrador Sea Water to the Irminger and Iceland basins, *Geophys. Res. Lett.*, *34*, L10602, doi:10.1029/2006GL028999.